









RESEARCH ARTICLE | MAY 02 2024

# Polarization-controlled unidirectional lattice plasmon modes via a multipolar plasmonic metasurface

Seyedehniousha Mousavi ; Muhammad Abdullah Butt ; Zeinab Jafari ; Orad Reshef ; Robert W. Boyd ; Peter Banzer ; Israel De Leon  

 Check for updates

*Appl. Phys. Lett.* 124, 181703 (2024)


<https://doi.org/10.1063/5.0195583>




View Online




Export Citation




Nanotechnology & Materials Science




Optics & Photonics



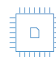
Impedance Analysis




Scanning Probe Microscopy



Sensors




Failure Analysis & Semiconductors



**Unlock the Full Spectrum.**  
From DC to 8.5 GHz.

Your Application. Measured.

[Find out more](#)



# Polarization-controlled unidirectional lattice plasmon modes via a multipolar plasmonic metasurface

Cite as: Appl. Phys. Lett. **124**, 181703 (2024); doi: [10.1063/5.0195583](https://doi.org/10.1063/5.0195583)

Submitted: 18 January 2024 · Accepted: 24 April 2024 ·

Published Online: 2 May 2024










View Online



Export Citation



CrossMark

Seyedehniousha Mousavi,<sup>1</sup>  Muhammad Abdullah Butt,<sup>2</sup>  Zeinab Jafari,<sup>1,a)</sup>  Orad Reshef,<sup>3,b),c)</sup>   
Robert W. Boyd,<sup>3,b),c)</sup>  Peter Banzer,<sup>2,b),d)</sup>  and Israel De Leon<sup>4,b),e),f)</sup> 

## AFFILIATIONS

<sup>1</sup>School of Engineering and Sciences, Tecnologico de Monterrey, Monterrey, Nuevo León 64849, Mexico

<sup>2</sup>Max Planck Institute for the Science of Light, Guenther-Scharowsky-Str. 1, Erlangen D-91058, Germany

<sup>3</sup>Department of Physics, University of Ottawa, Ottawa, Ontario K1N 6N5, Canada

<sup>4</sup>School of Electrical Engineering and Computer Science, University of Ottawa, Ottawa, Ontario K1N6N5, Canada

<sup>a)</sup>Also at: IMEC, Kapeldreef 75, Leuven 3001, Belgium.

<sup>b)</sup>Also at: Max Planck, University of Ottawa Center for Extreme and Quantum Photonics, University of Ottawa, Ottawa, Ontario K1N6N5, Canada.

<sup>c)</sup>Also at: The Institute of Optics, University of Rochester, Rochester, New York 14627, USA.

<sup>d)</sup>Also at: Institute of Physics, University of Graz, NAWI Graz, Universitätsplatz 5, 8010 Graz, Austria and Also at: Christian Doppler Laboratory for Structured Matter Based Sensing, Institute of Physics, Universitätsplatz 5, 8010 Graz, Austria.

<sup>e)</sup>Also at: School of Engineering and Sciences, Tecnologico de Monterrey, Monterrey, Nuevo León 64849, Mexico and Also at: ASML Netherlands B.V., De Run 6501, 5504 DR Veldhoven, The Netherlands.

<sup>f)</sup>Author to whom correspondence should be addressed: [ideleona@uottawa.ca](mailto:ideleona@uottawa.ca)

## ABSTRACT

Diffraction plasmonic metasurfaces offer the possibility of controlling the flow of light in flat optical systems through the excitation of lattice plasmon modes by a careful metasurface design. Nonetheless, a remaining challenge for this type of structure is the dynamic control of its optical properties via degrees of freedom, such as the polarization states of incoming light. In this report, we explain theoretically and demonstrate experimentally the polarization control over amplitude and propagation direction of lattice plasmon modes supported by a multipolar plasmonic metasurface. These unidirectional optical waves result from the coupling between near-field effects of individual meta-atoms and far-field effects originating from the lattice modes. The device operates over a broad wavelength range, maintaining its directional behavior and enabling it to operate also as a polarization-controlled directional diffraction grating, a power splitter, or an optical router for on-chip photonics applications.

Published under an exclusive license by AIP Publishing. <https://doi.org/10.1063/5.0195583>

The ability to manipulate light's behavior in two-dimensional systems through polarization control is key for the development of next-generation multifunctional planar photonic systems, wherein metasurfaces play a crucial role. Notably, recent advances in metasurface-based optical devices have revealed approaches to generate broadband and highly efficient optical beams.<sup>1</sup> Concurrently, investigations have explored frameworks for asymmetric polarization-locked devices<sup>2</sup> as well as efforts to investigate compact and efficient chiral mode converters.<sup>3</sup> Similarly, metasurface-based sensing and imaging technologies have made significant advances, with studies focusing on improving imaging polarimetry resolution

through different metalens configurations,<sup>4</sup> and advancements in terahertz chiral metasurface absorbers with improved circular dichroism holding promise for sensing applications.<sup>5</sup> Furthermore, metallic structures supporting surface plasmons (SPs) offer important advantages due to their intrinsic two-dimensional nature, capacity for subwavelength field confinement, and enhanced light-matter interactions.<sup>6,7</sup> In particular, two-dimensional arrays of plasmonic nanostructures (typically referred to as plasmonic metasurfaces) have been exploited in earlier works, for their narrow resonances near Rayleigh anomaly, which is a result of diffraction coupling of localized plasmons.<sup>8–10</sup>

Plasmonic metasurfaces enable engineering the optical properties of light.<sup>11–16</sup> Particularly, much effort has been devoted to exploring mechanisms for controlling light's propagation in metallic and dielectric films and complex metasurfaces, unveiling the rich physics governing the flow of optical fields in such systems.<sup>17–20</sup> Similarly, a spin-direction locking in SPs has been shown to enable spin-selective directional propagation of SP waves in flat metallic surfaces.<sup>21–24</sup> Various plasmonic systems have been demonstrated for controlling the propagation of light using degrees of freedom, such as the field's amplitude, phase, and other optical properties.<sup>25–33</sup> Coupling of near-field and far-field effects helps us to enhance the overall optical response. For instance, the distance between individual meta-atoms when comparable to the wavelength of incident light can make a metasurface support delocalized collective excitations bound to the metasurface. Such modes, termed *lattice plasmon modes* (LPMs),<sup>34,35</sup> propagate on the plane of the metasurface with relatively low losses, enabled by phase-matched radiative coupling of the localized plasmon modes supported by the individual nanoparticles or meta-atoms.

Despite the significant research on lattice plasmon modes (LPMs) and their applications,<sup>36–40</sup> a major challenge remains, the limitations of current methods for controlling LPM directionality using light polarization over a broad wavelength range. While diffractive plasmonic metasurfaces, like those reported in Ref. 38, have shown promise in achieving asymmetric transmission for opposing circular polarization states, recent advancements in the metasurface design offer even greater potential to finer control over light propagation and directionality. Notably, holographic metasurfaces, for instance, utilize designed patterns to tailor the wavefront of emitted light, achieving high efficiency.<sup>41</sup> On the other hand, nano-antenna metasurfaces boast near-perfect light-harvesting efficiencies.<sup>42</sup> Nonetheless, their intricate metasurface configuration can introduce complexities in design and fabrication. In this work, we now theoretically and experimentally demonstrate a metasurface design that acts as a tunable, polarization-controlled directional diffraction grating, enabling on-demand control of LPM directionality over a broad wavelength range. Such large broadband tuning eliminates the need for complex wavelength-specific designs and enables a wide range of applications across the electromagnetic spectrum.

The plasmonic metasurface under investigation is illustrated in Fig. 1(a). It consists of a square array of U-shaped gold split-ring resonators (SRRs) with a lattice spacing of  $a = 600$  nm. The SRR array is fabricated on a glass substrate with a refractive index  $n = 1.5$ . Index-matching oil is used to obtain a symmetric cladding environment around the array. The illumination field is a plane wave propagating in the  $(x, z)$  plane, with its wavevector aligned at an angle  $\theta$  with respect to the normal of the metasurface. We study first the case for  $s$  and  $p$  polarized illumination, defined by the polarization unit vectors  $\hat{s} = \hat{y}$  and  $\hat{p} = \cos \theta \hat{x} - \sin \theta \hat{z}$ . Later, we will build on this analysis to study the response of elliptical and circular polarization states.

The isolated SRR nanoparticle can support various multipolar localized plasmon resonances when illuminated with linearly polarized light. Two of those resonances are characterized by electric dipole (ED) and electric quadrupole (EQ) charge distributions.<sup>38</sup> We are mainly interested in these two modes as they are excited at a wavelength close to Rayleigh anomaly wavelength (900 nm) as a key condition to enable polarization selective propagation of our LPMs. Figure 1(b) shows a schematic representation of the charge distribution of

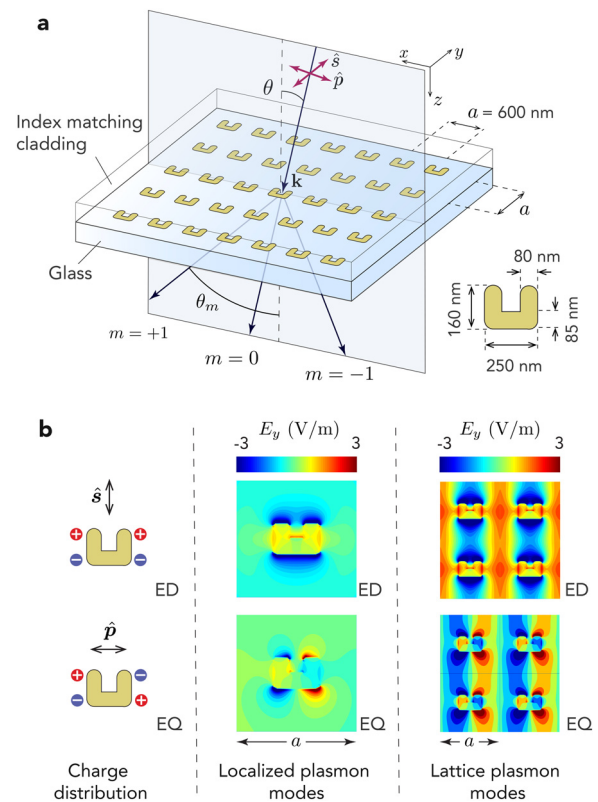


**FIG. 1.** (a) Schematic illustration of the metasurface under investigation and the optical excitation arrangement. Inset: dimensions of the SRR meta-atoms. (b) Schematic illustration of the charge distribution for the ED and EQ localized plasmons supported by the SRR (left panel); real  $E_y$  field component for the respective localized plasmons modes of the isolated SRR (center panel); and real  $E_y$  field component for the respective LPMs (right panel).

two such resonances (left panel) along with the distribution of their  $y$  electric field component (center panel), obtained numerically using the finite-difference time-domain (FDTD) method for normal incidence illumination. The ED resonance is excited with normally incident  $\hat{s}$ -polarization, and its spectrum is centered at a wavelength of 960 nm, while the EQ resonance is excited with normally incident  $\hat{p}$ -polarization and exhibits a central wavelength of 900 nm, overlapping partially with the spectrum of the ED resonance.

The SRR array supports diffraction orders in the planes of periodicity when the optical wavelength is on the order of the lattice spacing. We consider only diffraction orders lying in the  $(x, z)$  plane, whose diffraction angles  $\theta_m$  are given by the well-known grating equation as follows:

$$\sin \theta_m = \sin \theta + mG/k, \quad (1)$$

where the index  $m = 0, \pm 1, \pm 2, \dots$  identifies the diffraction order,  $G = 2\pi/a$  is the reciprocal lattice constant, and  $k = 2\pi/\lambda$  is the wavenumber of light in the medium with  $\lambda$  being the optical wavelength in vacuum. The zeroth diffraction order ( $m = 0$ ) corresponds to the non-diffracted transmission.

The condition at which the diffraction order's direction coincides with the plane of the array ( $\theta_m = \pm 90^\circ$ ) is referred to as the Rayleigh

anomaly (RA) condition. For the  $m$ th non-zero diffraction order, this anomaly occurs at the wavelength given as follows:<sup>43</sup>

$$\lambda_{\text{RA}}^m = \frac{an}{|m|} [1 - \text{sgn}(m) \sin \theta], \quad (2)$$

where  $\text{sgn}(\cdot)$  is the signum function. For values of  $\lambda_{\text{RA}}$  close to the nanoparticle's localized plasmons resonance, the array supports LPMs resulting from the diffractive coupling between nanoparticles.<sup>34</sup> The metasurface was designed to support two LPMs at a particular optical frequency, one for each of the SRR localized plasmon resonances. The LPM associated with ED resonance is excited by  $\hat{s}$ -polarized light, while the one associated with the EQ resonance is excited by  $\hat{p}$ -polarized light.

The propagation direction of both modes is restricted to the  $\pm x$  directions. This implies that the field components,  $E_\ell$  and  $H_\ell$ , responsible for carrying the energy through the lattice are those with  $\ell = y, z$ . However, a Poynting vector analysis reveals that the contribution of  $E_z$  and  $H_y$  is negligible (not shown here). Thus, in what follows, we simplify our discussion by making reference to the LPM's electric field as a scalar, considering only its main electric field component  $E_y$ , and dropping the subscript  $y$  in our notation.

The right panel of Fig. 1(b) shows the real part of the main electric field component of the ED and EQ LPMs,  $E_{\text{ED}}$  and  $E_{\text{EQ}}$ , obtained from FDTD simulations using a normally incident illumination at  $\lambda = 968$  nm. Both fields are standing waves generated by LPMs propagating in opposite directions, as expected for  $\theta = 0$  [see Eq. (2)]. Observe that  $E_{\text{ED}}$  and  $E_{\text{EQ}}$  have very similar spatial distributions, but they are shifted by a quarter of an optical cycle. This key feature is the result of LPMs maintaining the field symmetry of their respective localized plasmon modes.<sup>38</sup> Our metasurface design exploits this field symmetry to generate a set of modes with a unidirectional propagation through constructive and destructive interference induced by carefully selecting the polarization state of the incident light.

Consider an incident optical field with an elliptical polarization state given by

$$\hat{e} = \hat{s} \cos \varphi + i \hat{p} \sin \varphi, \quad (3)$$

where  $\varphi$  can take values between  $-\pi$  and  $\pi$ . The polarization vector describes  $\hat{s}$  ( $\hat{p}$ ) polarization for  $\varphi = 0$  ( $\varphi = \pm\pi$ ) and right-handed (left-handed) elliptical polarization for  $\varphi > 0$  ( $\varphi < 0$ ). The special cases of right-handed circular polarization (RCP) and left-handed circular polarization (LCP) correspond to  $\varphi = \pi/2$  and  $\varphi = -\pi/2$ , respectively. Such an optical field excites a linear superposition of ED and EQ LPMs given by  $E_{\hat{e}} = \cos \varphi E_{\text{ED}} + i \sin \varphi E_{\text{EQ}}$ . This is because the ED (EQ) LPMs are excited solely by  $s$  ( $p$ ) polarization.<sup>38</sup> As a result, the phase angle  $\varphi$  allows us to modulate the relative contributions of ED and EQ modes. Assuming for simplicity that  $E_{\text{EQ}}$  is identical to  $E_{\text{ED}}$  but dephased by a quarter of an optical cycle, and expressing these fields as plane wave expansions, we can write the electric field distribution of  $E_{\hat{e}}$  in the  $(x, y)$  plane as (see the supplementary material)

$$E_{\hat{e}}(x, y) = E_+(x, y) + E_-(x, y), \quad (4)$$

where

$$E_+(x, y) = A_+(\varphi) \sum_{m>0} c_m(y; k_x) e^{imGx} e^{ik_x x}, \quad (5)$$

$$E_-(x, y) = A_-(\varphi) \sum_{m<0} c_m(y; k_x) e^{imGx} e^{ik_x x}. \quad (6)$$

Here,  $m$  has the same meaning as in Eq. (1),  $c_m$  are Fourier coefficients of the plane wave expansion of  $E_{\text{ED}}$ ,  $k_x$  is the LPM wavenumber, and  $A_\pm = \cos \varphi \pm \sin \varphi$ . The  $E_\pm$  functions represent the main electric field component of two LPMs formed through the interference of the ED and EQ LPMs. Since their fields are associated with diffraction orders  $m$  with opposite signs, these modes propagate in opposite directions. Thus, Eq. (4) states that LPMs excited by  $\hat{e}$ -polarized light consists of two counter-propagating modes with polarization-dependent amplitudes given by  $A_\pm$ .

As expected, for  $\hat{s}$ - and  $\hat{p}$ -polarized illumination, the field given by Eq. (4) describes waves propagating in both  $\pm x$  directions with equal amplitudes ( $|A_+| = |A_-| = 1$ ). However, for RCP and LCP, one of the two counter-propagating fields vanishes resulting in LPMs with unidirectional propagation ( $A_- = 0$  for RCP and  $A_+ = 0$  for LCP). This behavior is confirmed by the FDTD calculations reported in Figs. 2(a) and 2(b), which show the transmittance spectrum of the metasurface for various polarization states as a function of the incidence angle (see the supplementary material for further details of the simulation). The results show that LPMs excited by  $\hat{s}$ - and  $\hat{p}$ -polarized light are associated with both  $m = \pm 1$  RAs (superimposed dashed lines) and hence define modes with plane wave components propagating in both  $\pm x$  directions for a given value of  $k_x$ . On the other hand, LPMs excited with RCP and LCP are associated with only one RA, defining modes with unidirectional propagation. In particular, LPMs excited with RCP (LCP) propagate in the direction of the  $E_+$  ( $E_-$ ) field. The propagation direction of these LPMs is determined from the sign of their group velocities,  $v_g = \partial\omega/\partial k_x$ . The group velocity  $v_g$  is calculated from the data in Fig. 2(b) using  $k_x = k \sin \theta$  and  $\omega = 2\pi c/\lambda$ . The results, plotted in Fig. 2(c) and normalized to the speed of light in a vacuum ( $c$ ), indicate that LPMs excited with RCP (and hence  $E_+$ ) propagate in the  $+x$  direction, while LPMs excited with LCP (and hence  $E_-$ ) propagate in the  $-x$  direction.

Since the amplitudes of the fields  $E_+$  and  $E_-$  are set by the parameter  $\varphi$ , the power of an incident  $\hat{e}$ -polarized optical field is split into counter-propagating LPMs with power splitting ratios (PSR) controlled by the ellipticity of the polarization state. In particular, for non-overlapping counter-propagating LPMs excited at normal incidence, the PSR is given by  $|E_+|^2/(|E_+|^2 + |E_-|^2)$  and is given by (see the supplementary material),

$$\text{PSR}_\pm = \frac{1}{2} \pm \left( \frac{2\kappa - 1}{2} \right) \sin 2\varphi, \quad (7)$$

where  $\kappa$  is a constant that quantifies the efficiency of power splitting and represents the fraction of the coupled power propagating in the "correct" direction. Note that the simple model that we have described here assumes the perfect interference of LPMs. Based on such a model,  $\kappa = 1$ . However, we have added this constant following a phenomenological approach to describe the experimental results reported above.

The metasurface is fabricated on  $\sim 100$   $\mu\text{m}$ -thick N-BK7 glass substrate with each SRR array having a dimension of roughly  $400 \times 400$   $\mu\text{m}$ . The metasurface was fabricated using electron beam (e-beam) lithography of a bilayer PMMA resist followed by a standard metal liftoff technique according to the design specifications mentioned earlier. A fused silica substrate was used and the SRR pattern was defined on the substrate using e-beam lithography through a commercial conductive polymer. The gold was deposited on the glass substrate using thermal evaporation with a thickness of 42.3 nm and a

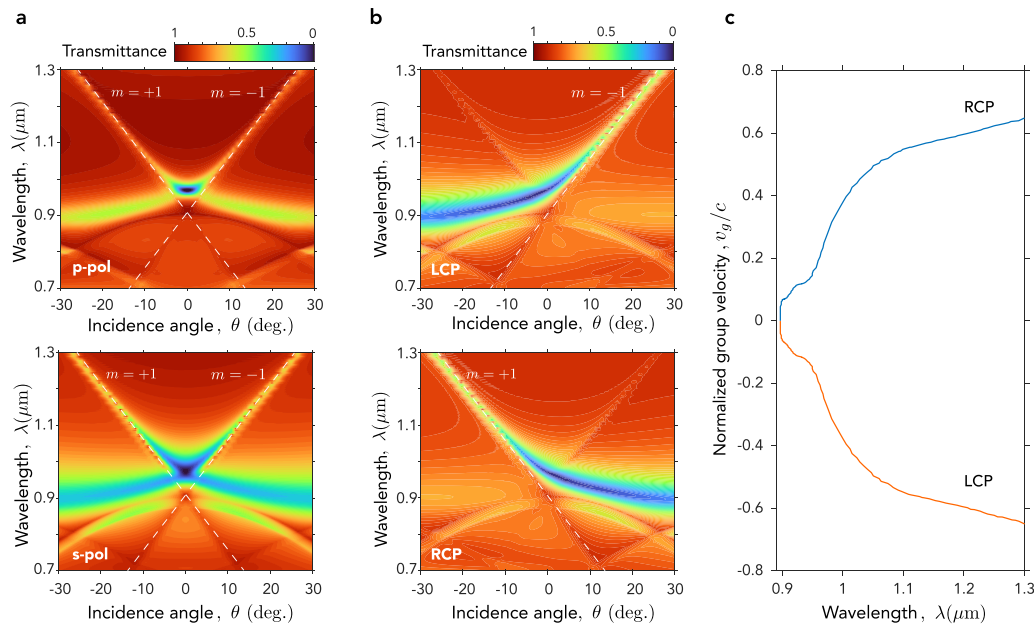


**FIG. 2.** (a) Transmittance spectra of the metasurface calculated for  $\hat{s}$  and  $\hat{p}$  polarized light as a function of the incidence angle  $\theta$ . The Rayleigh anomaly (RA) conditions are shown as white dashed lines. (b) Same as (a) but for RCP and LCP illumination, respectively. (c) Group velocity of LPMs excited with RCP and LCP light normalized to the speed of light in vacuum. All the results are obtained from FDTD simulations.

deposition rate of 0.05 nm/s. The final silica cladding layer was deposited via sputtering. To make the necessary corrections for corner rounding, a mask was designed by incorporating a shape correction proximity error correction.<sup>44</sup> A scanning electron micrograph of the fabricated sample is shown in the inset of Fig. 3(a).

The sample is characterized using the experimental arrangement schematically shown in Fig. 3(a). The light source is a tunable Ti:sapphire pulsed laser (100 fs pulse width, 80 MHz repetition rate). The laser light is linearly polarized and a half-waveplate (HWP) followed by a quarter-waveplate (QWP) is used to control its polarization state on the plane of the sample. The beam is focused onto the sample using a low numerical aperture (NA = 0.2125) lens with a focal length of 60 mm. The focused beam at the sample has a Gaussian profile with a full-width-at-half-maximum size of approximately 30  $\mu\text{m}$ . The transmitted light is then collected by a 100 $\times$  oil-immersion microscope objective with NA = 1.3 and directed toward the optical detection system. The experimental data reported were obtained by repeating each set of experimental measurements five times. The value reported represents the mean value, and the error bars show the minimum and maximum values obtained.

For measurements of the transmittance spectrum, the optical detection system consists of a lens followed by a calibrated silicon photodetector. The HWP is used to align the laser polarization to the y axis of the sample, and the QWP is adjusted to generate a circularly polarized state. Figure 3(b) shows the measured transmittance (symbols) and the respective FDTD calculation (solid line) for RCP illumination at normal incidence. A similar result is obtained for LCP illumination (data not shown). A good agreement is observed between

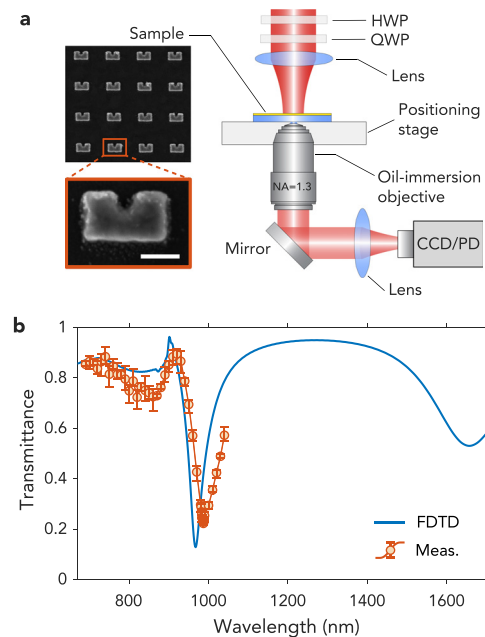


**FIG. 3.** (a) Schematic diagram of the experimental setup. Linearly polarized light from a tunable laser is used to perform measurements in the 690–1040 nm spectral range. HWP: Half-waveplate; QWP: Quarter waveplate; CCD/PD: CCD camera or photodetector. Inset: Scanning electron micrograph of the fabricated SRR metasurface; the scale bar is 100 nm. (b) Simulated and experimental transmittance spectrum of the SRR metasurface for normally incident RCP light.

the numerical calculations and the measurements, confirming the proper operation of the sample. The transmittance minimum, located at  $\lambda = 987$  nm, is red-shifted by 20 nm from the numerical result and the measured linewidth is slightly larger than the one obtained numerically. These discrepancies can be attributed to sample imperfections due to the fabrication process and to a mismatch between the substrate's refractive index and oil cladding.

To experimentally characterize the directional excitation and power splitting of the direction LPMs supported by our metasurface, we employ leakage radiation microscopy (LRM).<sup>45–51</sup> For this, the bottom lens in Fig. 3(a) is adjusted to image the plane of the sample on a CCD camera. The HWP is used to align the laser polarization to the  $y$  axis of the sample, and the QWP is used to generate the polarization state in Eq. (3) by rotating its fast axis by an angle  $\varphi$  with respect to the  $y$  axis of the sample. Figures 4(a)–4(c) show LRM images of the LPMs excited at normal incidence with circular and linear polarization states and a wavelength of  $\lambda = 987$  nm. The figures show the normalized intensity on a logarithmic scale to clearly visualize the weak leakage radiation despite the relatively strong zeroth order transmission (marked with a dashed circle in the images). The results confirm our previous theoretical and numerical analysis [Figs. 2(b) and 2(c)], showing bidirectional excitation of nearly equal LPMs by  $\hat{s}$ -polarized light

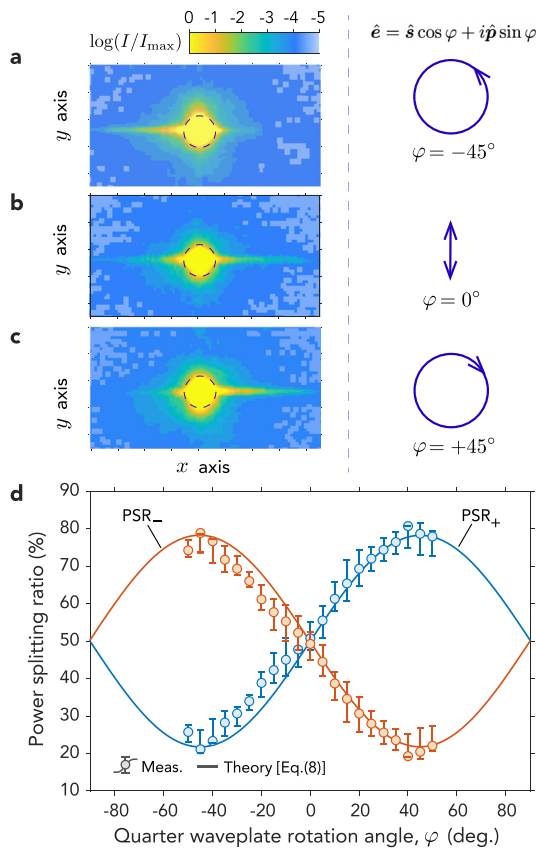


**FIG. 4.** (a)–(c) LRM images of the intensity distribution at the sample plane obtained at  $\lambda = 987$  nm for the various polarization states generated by varying the QWP rotation angle,  $\varphi$ . (d) Theoretical (solid lines) and experimental (data points) power splitting ratio of LPMs as a function of  $\varphi$ .

and unidirectional excitation of LPMs by RCP and LCP light. However, we observe in Figs. 4(a) and 4(c) that the unidirectional excitation efficiency is not 100%, as a relatively small portion of the field remains propagating in the wrong direction. We quantify the LPM power splitting based on the obtained LRM images. For this, we integrate the LPM intensity distribution on the  $+x$  and  $-x$  regions of the image (excluding the pixels within the dashed circles) and divide it over the sum. Figure 4(d) shows the percentage of the total power carried by the LPMs in the  $+x$  (blue curve) and  $-x$  (orange curve) directions as a function of the QWP rotation angle,  $\varphi$ . For linear polarization, we obtain nearly 50% of power splitting between the two LPMs. The splitting ratio increases (decreases) for the LPM propagating in the  $+x$  ( $-x$ ) direction as  $\varphi$  increases (decreases). For  $\varphi = \pm 45^\circ$ , corresponding to circular polarization, the PSR is approximately 80% – 20%. The solid curves in Fig. 4(d) show the theoretical PSRs obtained with Eq. (7) using  $\kappa = 0.78$ . We observe a very good agreement with the measured data, suggesting that our simple theoretical model describes well the underlying physical phenomenon.

Investigating the directional response of our metasurface within its diffraction orders, we observe, as per Eq. (1), diffraction orders appear in transmission with angles  $\theta_m$  for wavelengths  $\lambda < \lambda_{RA}^m$ . Interestingly, we observe that such diffraction orders also exhibit a polarization-controlled directional behavior over a broad range, which was only limited by the laser source and collection optics used for the experiment.

At normal incidence, the  $m = \pm 1$  diffraction orders can couple to the far field for wavelengths  $\lambda < 909$  nm according to Eq. (1). However, because of the limited NA of our optical collection system, the detection was limited to these diffraction orders only for  $\theta_{\pm 1} < 60^\circ$ , which corresponds to wavelengths  $\lambda < 780$  nm. Figure 5(a) presents differential images of the Fourier plane for circularly polarized illumination at normal incidence for various wavelengths in this range. The images are obtained by performing a pixel-by-pixel subtraction of the image recorded for RCP and LCP illumination for each wavelength. The directional diffraction response of the metasurface is apparent from these images as the light is coupled to different diffraction orders ( $+1$  or  $-1$ ) as the handedness is changed (RCP or LCP).

We define the directionality efficiency of the first diffraction order for RCP (LCP) illumination as the power in the  $m = +1$  ( $m = -1$ ) diffraction order divided by the total power of the first diffraction orders,

$$\eta_{\pm} = \frac{P_{\pm 1}}{P_{+1} + P_{-1}}, \quad (8)$$

where  $P_{\pm 1}$  is the power carried by the  $m = \pm 1$  diffraction order. Figure 5(b) shows the experimental values (symbols) and FDTD calculation (dashed curves) obtained for  $\eta_{\pm}$  for various wavelengths. The numerical and experimental values are in good agreement. The maximum directionality efficiency obtained is  $\eta_{\pm} \approx 90\%$  and occurs for wavelengths around 770 nm. The minimum value is  $\eta_{\pm} \approx 70\%$  at 690 nm. We could not measure the response for shorter wavelengths due to the limited tuning range of our laser; however, it should be noted that at such shorter wavelengths ( $\lambda < 780$  nm) LPMs are not supported and we are in fact observing the radiative modes diffracting to out-of-plane.

In conclusion, we have demonstrated theoretically and experimentally that the directionality of the modes is enabled by near-field

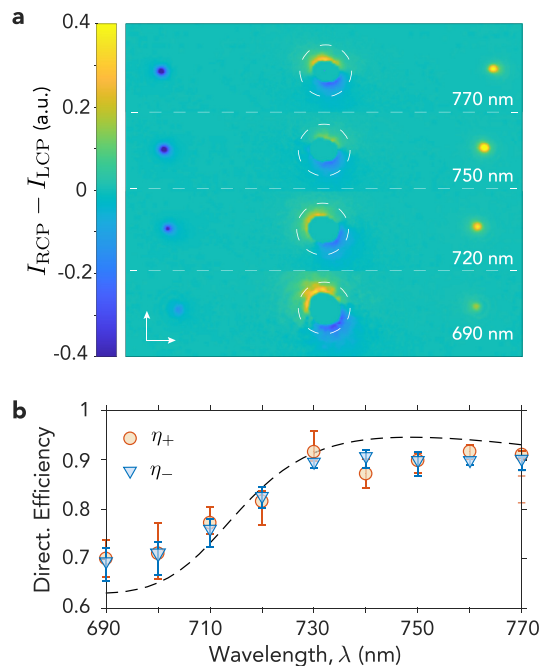


**FIG. 5.** (a) Pixel-by-pixel difference of the experimental Fourier-space images recorded in transmission when illuminating the metasurface at normal incidence with RCP and LCP light of various wavelengths. The zeroth (central circle), +1 (right) and -1 (left) diffraction are shown in the images. (b) Experimental and simulated plots of the directionality efficiency defined in Eq. (8).

interference between plasmonic modes with even (dipolar) and odd (quadrupole) symmetries. We show that the amount of power carried by LPMs in a particular direction is controlled by the polarization ellipticity of the illumination. This allows the structure to operate as an ultrathin polarization-controlled power splitter or variable-power optical router. We also show that the metasurface preserves the directional behavior for radiative diffraction orders and measured a polarization-dependent directionality efficiency of up to 90% efficiency in the first diffraction order. Given the inherited frequency tunability of LPMs, this device is capable of operating over a broad wavelength range by simply controlling the angle of incidence of the illumination source. Our work paves the way for developing polarization-controlled diffractive metasurfaces for applications with sophisticated functionalities, such as ultrathin polarization-controlled optical routers, tunable polarization filters, and directional plasmonic lasers.

See the supplementary material for details regarding the mathematical derivation of Eqs. (4)–(7) included in the main text and details of the simulation parameters used in this work.

This work was supported by Federico Baur Endowed Chair in Nanotechnology; the Natural Sciences and Engineering Research Council of Canada; the Canada Research Chairs; the Defense Advanced Research Projects Agency (W911NF-18-1-0369); the Army Research Office (W911NF-18-1-0337); the Office of Naval Research (N00014-20-1-2558); the National Science Foundation (2138174); the U.S. Department of Energy; Austrian Federal

Ministry of Labour and Economy; the National Foundation for Research, Technology and Development; and the Christian Doppler Research Association.

## AUTHOR DECLARATIONS

### Conflict of Interest

The authors have no conflicts to disclose.

### Author Contributions

**Seyedehtiousha Mousavi:** Software (equal); Validation (equal); Visualization (lead); Writing – original draft (lead); Writing – review & editing (equal). **Muhammad Abdullah Butt:** Supervision (supporting); Writing – review & editing (equal). **Zeinab Jafari:** Software (equal); Supervision (equal); Writing – review & editing (equal). **Orad Reshef:** Resources (equal); Writing – review & editing (supporting). **Robert W. Boyd:** Conceptualization (equal); Supervision (supporting). **Peter Banzer:** Conceptualization (equal); Resources (supporting); Supervision (supporting); Validation (equal); Writing – review & editing (equal). **Israel De Leon:** Conceptualization (equal); Funding acquisition (lead); Project administration (equal); Resources (equal); Supervision (lead); Validation (equal); Writing – original draft (equal); Writing – review & editing (equal).

## DATA AVAILABILITY

The data that support the findings of this study are available from the corresponding author upon reasonable request.

## REFERENCES

- Z. Ju, J. Wen, L. Shi, B. Yu, M. Deng, D. Zhang, W. Hao, J. Wang, S. Chen, and L. Chen, “Ultra-broadband high-efficiency airy optical beams generated with all-silicon metasurfaces,” *Adv. Opt. Mater.* **9**, 2001284 (2021).
- A. Li, W. Chen, H. Wei, G. Lu, A. Alù, C.-W. Qiu, and L. Chen, “Riemann-encircling exceptional points for efficient asymmetric polarization-locked devices,” *Phys. Rev. Lett.* **129**, 127401 (2022).
- X. Shu, A. Li, G. Hu, J. Wang, A. Alù, and L. Chen, “Fast encircling of an exceptional point for highly efficient and compact chiral mode converters,” *Nat. Commun.* **13**, 2123 (2022).
- Z. Huang, Y. Zheng, J. Li, Y. Cheng, J. Wang, Z.-K. Zhou, and L. Chen, “High-resolution metalens imaging polarimetry,” *Nano Lett.* **23**, 10991–10997 (2023).
- C. Rong, B. Cai, Y. Cheng, F. Chen, H. Luo, and X. Li, “Dual-band terahertz chiral metasurface absorber with enhanced circular dichroism based on temperature-tunable InSb for sensing applications,” *Phys. Chem. Chem. Phys.* **26**, 5579 (2024).
- S. A. Maier, *Plasmonics: Fundamentals and Applications* (Springer, 2007), Vol. 1.
- L. Novotny and B. Hecht, *Principles of Nano-Optics* (Cambridge university Press, 2012).
- V. G. Kravets, F. Schedin, and A. N. Grigorenko, “Extremely narrow plasmon resonances based on diffraction coupling of localized plasmons in arrays of metallic nanoparticles,” *Phys. Rev. Lett.* **101**, 087403 (2008).
- B. Auguié and W. L. Barnes, “Collective resonances in gold nanoparticle arrays,” *Phys. Rev. Lett.* **101**, 143902 (2008).
- Y. Chu, E. Schonbrun, T. Yang, and K. B. Crozier, “Experimental observation of narrow surface plasmon resonances in gold nanoparticle arrays,” *Appl. Phys. Lett.* **93**, 181108 (2008).
- H.-T. Chen, A. J. Taylor, and N. Yu, “A review of metasurfaces: Physics and applications,” *Rep. Prog. Phys.* **79**, 076401 (2016).
- K. Du, H. Barkaoui, X. Zhang, L. Jin, Q. Song, and S. Xiao, “Optical metasurfaces towards multifunctionality and tunability,” *Nanophotonics* **11**, 1761–1781 (2022).

- <sup>13</sup>E. S. A. Goerlitzer, R. Mohammadi, S. Nechayev, K. Volk, M. Rey, P. Banzer, M. Karg, and N. Vogel, "Chiral surface lattice resonances," *Adv. Mater.* **32**, 2001330 (2020).
- <sup>14</sup>L. Zhang, S. Mei, K. Huang, and C.-W. Qiu, "Advances in full control of electromagnetic waves with metasurfaces," *Adv. Opt. Mater.* **4**, 818–833 (2016).
- <sup>15</sup>P. Genevet, F. Capasso, F. Aieta, M. Khorasaninejad, and R. Devlin, "Recent advances in planar optics: From plasmonic to dielectric metasurfaces," *Optica* **4**, 139–152 (2017).
- <sup>16</sup>A. V. Kildishev, A. Boltasseva, and V. M. Shalaev, "Planar photonics with metasurfaces," *Science* **339**, 1232009 (2013).
- <sup>17</sup>K. Y. Bliokh, F. J. Rodríguez-Fortuño, F. Nori, and A. V. Zayats, "Spin-orbit interactions of light," *Nat. Photonics* **9**, 796–808 (2015).
- <sup>18</sup>N. Shitrit, I. Yulevich, E. Maguid, D. Ozeri, D. Veksler, V. Kleiner, and E. Hasman, "Spin-optical metamaterial route to spin-controlled photonics," *Science* **340**, 724–726 (2013).
- <sup>19</sup>N. Yu, P. Genevet, M. A. Kats, F. Aieta, J.-P. Tetienne, F. Capasso, and Z. Gaburro, "Light propagation with phase discontinuities: Generalized laws of reflection and refraction," *Science* **334**, 333–337 (2011).
- <sup>20</sup>J. Lin, J. P. B. Mueller, Q. Wang, G. Yuan, N. Antoniou, X.-C. Yuan, and F. Capasso, "Polarization-controlled tunable directional coupling of surface plasmon polaritons," *Science* **340**, 331–334 (2013).
- <sup>21</sup>M. Neugebauer, T. Bauer, P. Banzer, and G. Leuchs, "Polarization tailored light driven directional optical nanobeacon," *Nano Lett.* **14**, 2546–2551 (2014).
- <sup>22</sup>K. Y. Bliokh, D. Smirnova, and F. Nori, "Quantum spin Hall effect of light," *Science* **348**, 1448–1451 (2015).
- <sup>23</sup>F. J. Rodríguez-Fortuño, G. Marino, P. Ginzburg, D. O'Connor, A. Martínez, G. A. Wurtz, and A. V. Zayats, "Near-field interference for the unidirectional excitation of electromagnetic guided modes," *Science* **340**, 328–330 (2013).
- <sup>24</sup>A. Aiello, P. Banzer, M. Neugebauer, and G. Leuchs, "From transverse angular momentum to photonic wheels," *Nat. Photonics* **9**, 789–795 (2015).
- <sup>25</sup>H. Mühlender, P. Georgi, N. Pholchai, L. Huang, G. Li, S. Zhang, and T. Zentgraf, "Amplitude- and phase-controlled surface plasmon polariton excitation with metasurfaces," *ACS Photonics* **3**, 124–129 (2016).
- <sup>26</sup>F. López-Tejeda, S. G. Rodrigo, L. Martín-Moreno *et al.*, "Efficient unidirectional nanoslit couplers for surface plasmons," *Nat. Phys.* **3**, 324–328 (2007).
- <sup>27</sup>Q. Jiang, A. Pham, M. Berthel, S. Huang, J. Bellessa, C. Genet, and A. Drezet, "Directional and singular surface plasmon generation in chiral and achiral nanostructures demonstrated by leakage radiation microscopy," *ACS Photonics* **3**, 1116–1124 (2016).
- <sup>28</sup>L. Huang, X. Chen, B. Bai, Q. Tan, G. Jin, T. Zentgraf, and S. Zhang, "Helicity dependent directional surface plasmon polariton excitation using a metasurface with interfacial phase discontinuity," *Light* **2**, e70 (2013).
- <sup>29</sup>F. Ding and S. I. Bozhevolnyi, "A review of unidirectional surface plasmon polariton metacouplers," *IEEE J. Sel. Top. Quantum Electron.* **25**, 4600611 (2019).
- <sup>30</sup>M. Khorasaninejad, W. Zhu, and K. Crozier, "Efficient polarization beam splitter pixels based on a dielectric metasurface," *Optica* **2**, 376–382 (2015).
- <sup>31</sup>D. Wang, Y. Hwang, Y. Dai, G. Si, S. Wei, D.-Y. Choi, D. E. Gómez, A. Mitchell, J. Lin, and X. Yuan, "Broadband high-efficiency chiral splitters and holograms from dielectric nanoarc metasurfaces," *Small* **15**, 1900483 (2019).
- <sup>32</sup>Q. Tu, J. Liu, S. Ke, B. Wang, and P. Lu, "Directional excitation of surface plasmon polaritons by circularly polarized vortex beams," *Plasmonics* **15**, 727–734 (2020).
- <sup>33</sup>S. Xiao, F. Zhong, H. Liu, S. Zhu, and J. Li, "Flexible coherent control of plasmonic spin-Hall effect," *Nat. Commun.* **6**, 8360 (2015).
- <sup>34</sup>V. G. Kravets, A. V. Kabashin, W. L. Barnes, and A. N. Grigorenko, "Plasmonic surface lattice resonances: A review of properties and applications," *Chem. Rev.* **118**, 5912–5951 (2018).
- <sup>35</sup>G. Vecchi, V. Giannini, and J. Gómez Rivas, "Surface modes in plasmonic crystals induced by diffractive coupling of nanoantennas," *Phys. Rev. B* **80**, 201401 (2009).
- <sup>36</sup>M. S. Bin-Alam, O. Reshef, Y. Mamchur, M. Z. Alam, G. Carlow, J. Upham, B. T. Sullivan, J.-M. Ménard, M. J. Huttunen, R. W. Boyd, and K. Dolgaleva, "Ultra-high-Q resonances in plasmonic metasurfaces," *Nat. Commun.* **12**, 974 (2021).
- <sup>37</sup>Y. Shen, J. Zhou, T. Liu, Y. Tao, R. Jiang, M. Liu, G. Xiao, J. Zhu, Z.-K. Zhou, X. Wang, C. Jin, and J. Wang, "Plasmonic gold mushroom arrays with refractive index sensing figures of merit approaching the theoretical limit," *Nat. Commun.* **4**, 2381 (2013).
- <sup>38</sup>I. De Leon, M. J. Horton, S. A. Schulz, J. Upham, P. Banzer, and R. W. Boyd, "Strong, spectrally-tunable chirality in diffractive metasurfaces," *Sci. Rep.* **5**(1), 13034 (2015).
- <sup>39</sup>A. Fernandez-Bravo, D. Wang, E. S. Barnard, A. Teitelboim, C. Tajon, J. Guan, G. C. Schatz, B. E. Cohen, E. M. Chan, P. J. Schuck, and T. W. Odom, "Ultralow-threshold, continuous-wave upconverting lasing from subwavelength plasmons," *Nat. Mater.* **18**, 1172–1176 (2019).
- <sup>40</sup>A. Yang, T. B. Hoang, M. Dridi, C. Deeb, M. H. Mikkelsen, G. C. Schatz, and T. W. Odom, "Real-time tunable lasing from plasmonic nanocavity arrays," *Nat. Commun.* **6**, 6939 (2015).
- <sup>41</sup>G. Li, B. P. Clarke, J.-K. So, K. F. MacDonald, and N. I. Zheludev, "Holographic free-electron light source," *Nat. Commun.* **7**, 13705 (2016).
- <sup>42</sup>J. Wang, G. Li, K. Ou, F. Yu, J. Chen, Z. Li, X. Chen, and W. Lu, "Controllable chiral emissions from free-electron driven plasmonic metasurfaces," *J. Phys. D* **54**, 105105 (2020).
- <sup>43</sup>S. Savoia, A. Ricciardi, A. Crescitelli, C. Granata, E. Esposito, V. Galdi, and A. Cusano, "Surface sensitivity of Rayleigh anomalies in metallic nanogratings," *Opt. Express* **21**, 23531 (2013).
- <sup>44</sup>S. A. Schulz, J. Upham, F. Bouchard, I. De Leon, E. Karimi, and R. W. Boyd, "Quantifying the impact of proximity error correction on plasmonic metasurfaces," *Opt. Mater. Express* **5**, 2798–2803 (2015).
- <sup>45</sup>S. Massenet, J. Grandidier, A. Bouhelier, G. Colas des Francs, L. Markey, J.-C. Weeber, A. Dereux, J. Renger, M. U. González, and R. Quidant, "Polymer-metal waveguides characterization by Fourier plane leakage radiation microscopy," *Appl. Phys. Lett.* **91**, 243102 (2007).
- <sup>46</sup>W. L. Barnes, A. Dereux, and T. W. Ebbesen, "Surface plasmon subwavelength optics," *Nature* **424**, 824–830 (2003).
- <sup>47</sup>K. A. Tetz, R. Rokitski, M. Nezhad, and Y. Fainman, "Excitation and direct imaging of surface plasmon polariton modes in a two-dimensional grating," *Appl. Phys. Lett.* **86**, 111110 (2005).
- <sup>48</sup>I. Radko, S. I. Bozhevolnyi, G. Brucoli, L. Martín-Moreno, F. García-Vidal, and A. Boltasseva, "Efficient unidirectional ridge excitation of surface plasmons," *Opt. Express* **17**, 7228–7232 (2009).
- <sup>49</sup>Y. Liu, S. Palomba, Y. Park, T. Zentgraf, X. Yin, and X. Zhang, "Compact magnetic antennas for directional excitation of surface plasmons," *Nano Lett.* **12**, 4853–4858 (2012).
- <sup>50</sup>E. Devaux, J.-Y. Laluet, B. Stein, C. Genet, T. Ebbesen, J.-C. Weeber, and A. Dereux, "Refractive micro-optical elements for surface plasmons: From classical to gradient index optics," *Opt. Express* **18**, 20610–20619 (2010).
- <sup>51</sup>A. Giannattasio and W. L. Barnes, "Direct observation of surface plasmon-polariton dispersion," *Opt. Express* **13**, 428–434 (2005).